IBGM Evaluatins Impact Factor 2017 – 2018
IRAQI BULLETIN OF GEOLOGY AND MINING
Arcif: 0.0755
GIF: 0.936

Iraqi Bulletin of Geology and Mining *Special Issue, No.8, 2019,*
The Geology and Economic Potential of Mineral Deposits and Occurrences of Iraq *p 41 – 63*

COPPER MINERALIZATION IN SELECTED AREAS OF KURDISTAN REGION, IRAQ: A REVIEW ON MINERALOGY AND GEOCHEMISTRY

Irfan O.M. Yara[1]

Received: 23/ 12/ 2018, Accepted: 05/ 08/ 2019
Keywords: Copper mineralization; Ore genesis; Ophilites; Kurdistan Region; Iraq

ABSTRACT

Copper mineralization in Iraq stretches along the northeast of Kurdistan Region, hosted by various rock units of the Mawat Ophiolites Complex and the Qandil Series. The mineralization in the Mawat Ophiolite is hosted by mafic igneous and associated quartz veins; meanwhile they are hosted in phyllite and marble in the Sharosh area. Two types of copper mineralization have been recognized by ore microscopy in the previous studies: disseminated and vein filling. Textural relationships among the minerals suggest three stages of mineralization: syngenetic, epigenetic and supergene enrichment. The dominant primary mineralization assemblage is represented by chalcopyrite, sphalerite, galena, pyrite, magnetite, and ilmenite. On the other hand, covellite, hematite, limonite goethite, tenorite, azurite, and malachite represent the supergene enrichment products. The Cu mineralization at the Mawat Ophiolite was formed from magmatic segregation and hydrothermal solution generated from tectonomagmatic activity. Mesothermal fluid system, with low to medium density and dilute NaCl-type, is the source of the mineralization at the Sharosh area. There is a promising potential to locate underground economic concentrations of copper in the Kurdistan Region based upon the evaluation of the wide spread copper supergene minerals at surface which indicate transportation of copper from subsurface sulfide mineralization to the supergene enrichment zone.

تمعدن النحاس في مناطق مختارة من إقليم كردستان، العراق: مراجعة في المعدنية والجيوكيمياء

عرفان عمر موسى ياره

المستخلص

تمتد تمعدنات النحاس فى العراق على طول الشمال الشرقي لإقليم كردستان، وتوجد في وحدات صخرية مختلفة من معقد أوفيوليت ماوات وسلسلة قنديل. توجد تمعدنات النحاس في اوفيوليت ماوات في صخور نارية قاعدية بالارتباط مع عروق من الكوارتز في حين انها توجد في صخور الفيليت والمرمر في منطقة شاروش. تم التعرف فى الدراسات السابقة على نوعين من تمعدنات النحاس حيث توجد هذه المعادن إما على شكل منتشر أوبشكل عروق موزعة فى وحدات صخرية مختلفة. على ضوء العلاقات النسيجية بين المعادن تم التعرف على ثلاث مراحل من التمعدن: اصلية المنشأ ولاحقة المنشأ ومنتجات الاغناء الفائق. من خلال الدراسات المجهريه للخامات تبين ان مجموعات التمعدن الغالبة فى أوفيوليت ماوات تتمثل بمعادن الجالكوبايريت والسفاليرايت والغالينا والبايرايت والماغنيتايت، وإلالمينايت وتمثل معادن الكوفيلايت

[1] Department of Geology, College of Science, University of Sulaimani, Iraq Qlyasan Campus, Sulaimaniyah-Kirkuk Main Road, e-mail: irfan.mosa@univsul.edu.iq

والهيماتيت والليمونيت والجوثايت والتينورايت والأزورايت والمالاخايت منتجات الاغناء الفائق. تكون التمعدن فى أوفيوليت ماوات من التجمعات الصهيرية والمحلول الحراري المائى الناتج عن النشاط التكتونى. فى حين ان التمعدن فى منطقة شاروش تكون فى درجة حرارة متوسطة بواسطة محلول كلوريد الصوديوم ذو كثافة متوسطة الى واطئة. هناك احتمالات مشجعه لوجود تراكيز اقتصادية للنحاس تحت الأرض فى إقليم كردستان العراق بناء على تقيم الشواهد المعدنية السطحيه التي تشير الى تحرر النحاس من معادنه تحت السطح نتيجة الاكسدة وانتقاله وتركيزه فى نطاق التركيز الفائق قرب سطح الارض.

INTRODUCTION

The Tethyan Metallogenic belt stretches from the Alps, through the Balkans, Turkey, Iraq, Iran, Pakistan, Tibet, Indochina, and ultimately into the southwest Pacific. It was formed during two major orogenic events, one in the early mid Mesozoic reflecting closure of the Paleo-Tethys Ocean, and the second in the early Cenozoic to Recent, reflecting the closure of the Neo-Tethys Ocean (Sengör and Yilmaz, 1981; Glennie, 2000; Ilbeyli *et al*., 2004). The Neo-Tethys Ocean was characterized by the presence of numerous small continental and island-arc fragments, which are now compacted between multiple sutures along the broad Tethyan Orogenic Belt. A diverse array of mineral deposit types is also associated with the belt (Richards *et al*., 2012). The central part of the Alpine-Himalayan Orogenic-Metallogenic Belt in Kurdistan Region hosts various metallic mineralizations in diverse rock units (Jasim and Goff, 2006). It remains one of the least understood and least explored geological domains of Kurdistan Region.

Kurdistan Region of Iraq is divided into two metallogenic zones on the basis of the tectonic framework and metallogenic features (Jassim and Goff, 2006 and Al-Bassam, 2007): **1)** The Imbricate Zone of the Western Zagros Fold-Thrust Belt, characterized by low-temperature hydrothermal vein and strata-bound, unmetamorphosed Zn, Pb, Cu, Ba, pyrite and siderite deposits and placer deposits of Cr, Fe, Mn, and Cu, and **(2)** The Zagros Suture Zone, characterized by magmatic, volcanic, metamorphic and hydrothermal types of ore minerals (Al-Bassam, 2013).

Occurrences of copper mineralization are widespread in the NE of Kurdistan Region, found as placer and secondary deposits in the Balambo-Tanjero Zone and magmatic, volcanic, metamorphic and hydrothermal types in the Zagros Suture Zone (Al-Bassam, 2013). Many of these occurrences are related to the serpentinized ultramafic rocks and gabbro of the Penjween, Mawat and Bulfat massifs (Fig.1). Quartz veins in Mawat and Qandil districts are occasionally hosting copper mineralization. Smirnov and Nelidov (1962) and Al-Hashimi and Al-Mehaidi (1975) reported many copper mineralization from the crush zone in gabbro SW of Korradawi Village and from granodiorites, pyroxenites and gabbros south of Konjrin Village. The mineralization consists of chalcopyrite, pyrite, malachite and azurite. Nahab *et al*. (1979) surveyed a part of the Waraz area, using five geophysical methods and concluded that the copper content ranges between (0.5 – 3.5 %). Furthermore, they studied the petrography of the rocks, and concluded that the most common rocks are metabasalt, metadiabase, quartzite, epidosite, keratophyr amphibolite and chlorite-schist. A detailed petrography, geochemistry and genesis of copper-iron mineralization and associated rocks in Waraz area has been done by Musa (2007). Hadi *et al.* (2010) studied the genesis of copper-iron mineralization and the associated rocks in the Waraz area. Yassin *et al*. (2015) studied copper ores in Mawat Ophiolite Complex (part of the Zagros Suture Zone) NE Iraq. Mirza *et al*. (2017); Mirza and Rashid (2018); and Yara and Mohammad (2018) studied the mineralogy, stable isotope, geochemistry and genesis of sulfide mineralization in the Zagros Suture rock units of the Kurdistan Region-Iraq. The present contribution is an overview of the copper mineralization

in the Mawat Ophiolite Complex and Qandil Series (Fig.1), based on previously published data. The main objective of this work is to clarify the mineralogy, geochemistry and genesis of copper mineralization in these areas. Unfortunately little is published on the mineral chemistry and geochemistry of Cu-sulfide minerals in the Mawat area, which kept this part lacking in the present contribution.

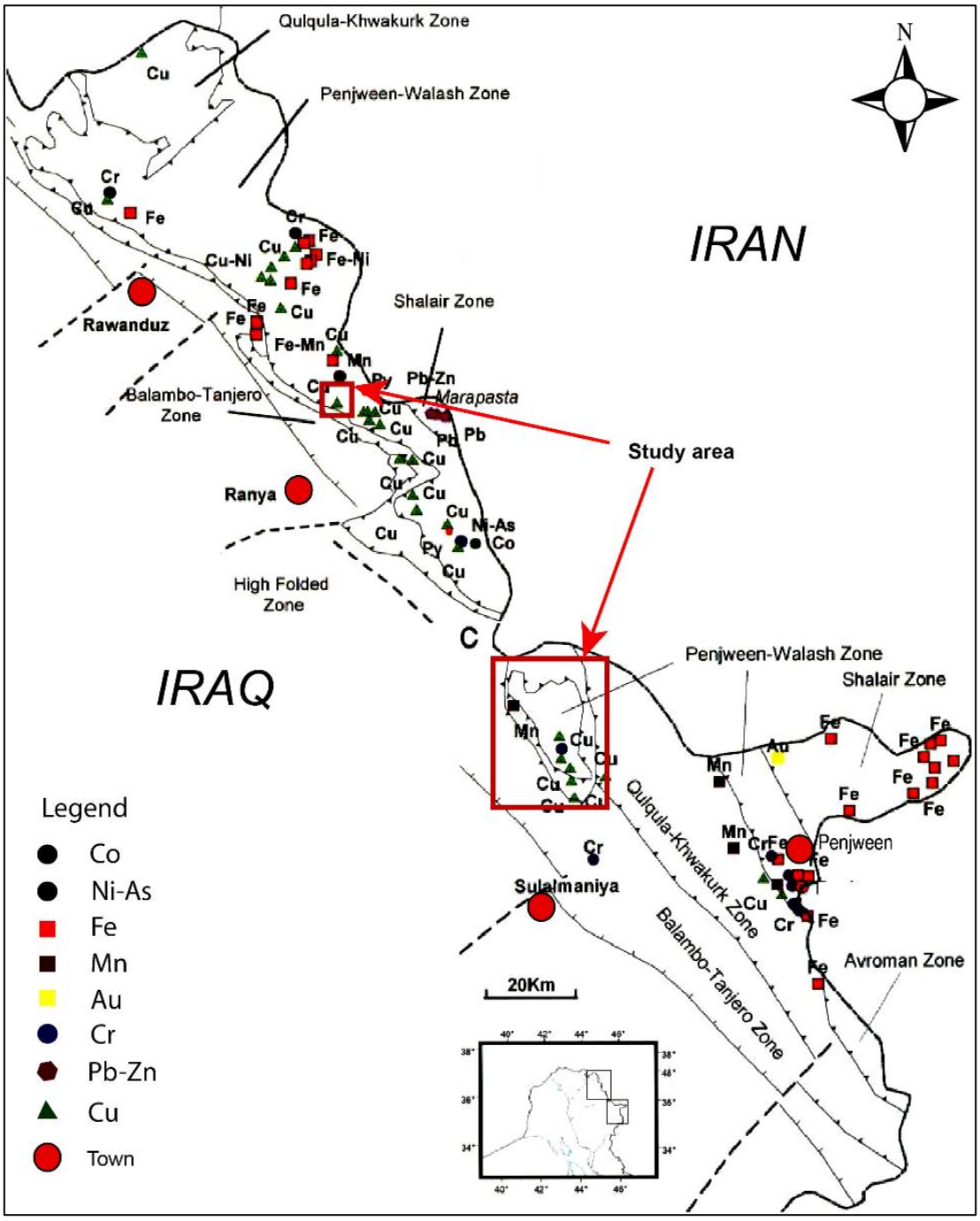

Fig.1: Location of the study area and distribution of the metallic mineralization in the eastern parts of Kurdistan Region, Iraq (after Vanecek, 1972)

GEOLOGICAL SETTING

The Zagros Mountains in the northeastern Iraq are located in the Alpine–Himalayan Mountain Range that extends in a NW – SE orientation (Fig.2). The Zagros Orogenic Belt consists of several main parallel tectonic zones: **1)** the Urumieh-Dokhtar Magmatic Arc (UDMA); **2)** the Sanandaj-Sirjan Zone (SSZ); **3)** the Zagros Fold-Thrust Belt (ZFB) and **4)** the Mesopotamian Foreland Basin (Fig.2b; Berberian and King, 1981; Alavi, 1994; Jassim and Goff, 2006). The Zagros Suture represents the northwestern part of the Zagros Orogenic Belt which extends approximately 1800 Km long zone of deformed crustal rocks from eastern Turkey through northeastern Iraq to western and southern Iran, ending at the Strait of Hormuz and into northern Oman (Moghadam and Stern, 2011, Fig.2). The Zagros Suture, formed as a result of a collision between the Arabian passive margin and the Iranian microcontinent active margin, is characterized by tectonic units of thrust sheets, which crop out in a (5 – 7) Km wide belt along the Iraqi – Iranian borders.

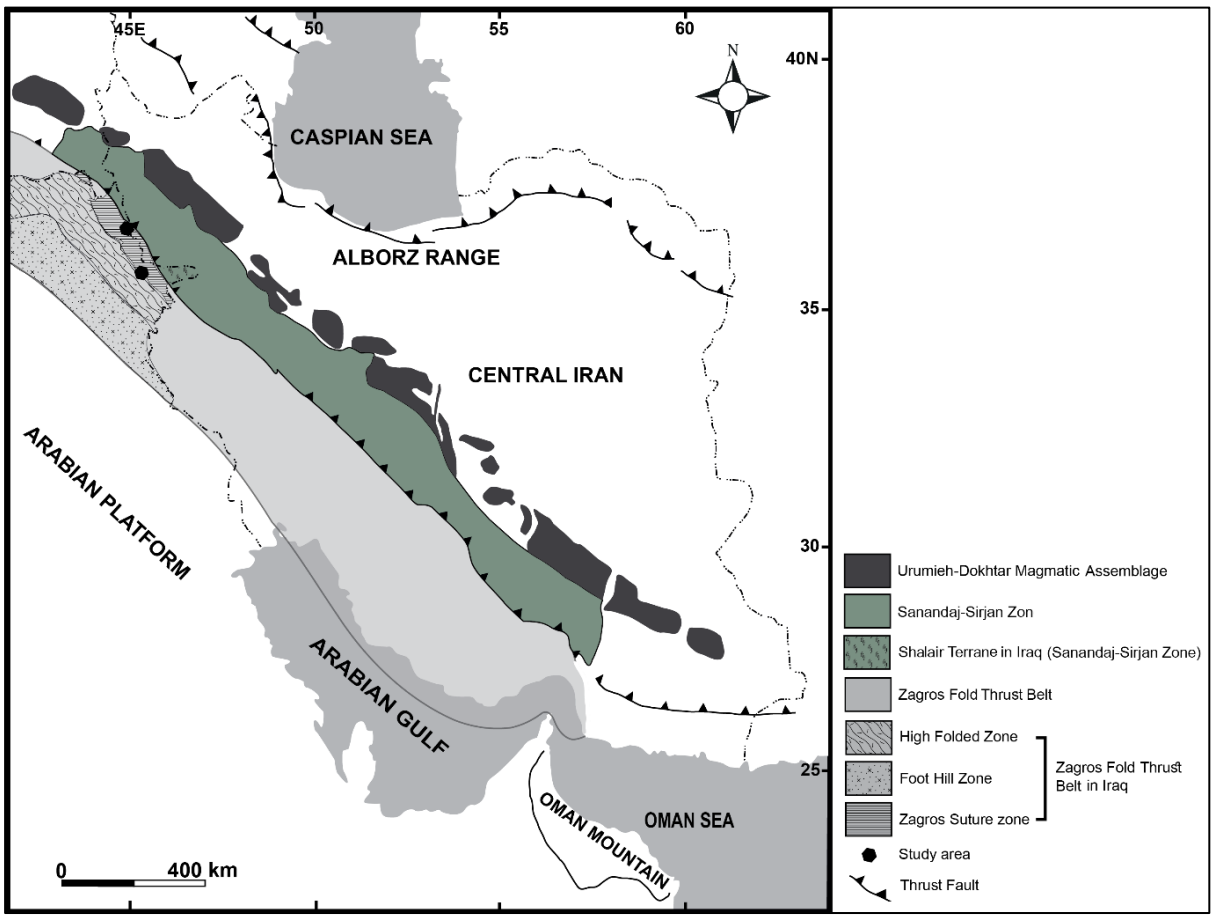

Fig.2: Zagros Orogenic Belt and tectonic map of Kurdistan Region of Iraq showing the main tectonic units and the location of the study area (after Jassim and Goff, 2006)

The units of the Zagros Suture Zone, formed within the Neo-Tethys, were thrusted over the Arabian Plate during two distinct phases of obduction and collision, during the Late Cretaceous and Mio-Pliocene (Jassim and Goff, 2006). The three tectonic zones identified within Iraq and reported in Jassim and Goff (2006) comprise from: **1)** The Qulqula – Khwakurk Zone with deformed radiolarites, carbonate turbidities and volcanics, and an upper thrust sheet of Triassic platform carbonates. These units were abducted onto the Arabian Plate

during the Late Cretaceous, **2)** The Penjween – Walash Zone with upper thrust sheets of metamorphosed volcanic, carbonates and pelitic rocks, and lower thrust sheets of non-metamorphosed Paleogene arc volcanic and fore-arc flysch and **3)** The Shalair Zone comprising thrust sheets of meta-pelitic and metacarbonates of Mesozoic age, Upper Cretaceous arc volcanics of Late Cretaceous age, and metamorphosed Paleozoic (?) rocks of the Sanandaj – Sirjan Zone.

The Penjween – Walash Zone consists of three thrust sheets: the structurally lowest is Naopurdan, the middle is Walash and the upper is Qandil (structurally highest). The upper Qandil thrust sheet contains basic igneous massifs, mostly along the SW margin. The massifs include, Penjween, Mawat, Bulfat and Pushtashan. The Penjween – Walash Zone represents the oceanic scope of the central part of the Neo-Tethys Ocean and includes metamorphosed volcanics and deposits of Cretaceous age. It also includes non-metamorphosed Paleogene fore-arc and volcanic arc rocks that formed during the final closure of the Neo-Tethys, therefore, it was considered a remnant of the ocean which was thrusted over the Arabian Plate during the Miocene – Pliocene time (Jassim and Goff, 2006). Most of the copper mineralization in the Kurdistan Region is classified as disseminated and vein filling (Musa, 2007; Yassin *et al*., 2015; Mirza *et al*., 2017; Mirza and Rashid, 2018; and Yara and Mohammad, 2018). The areas selected for this overview are located in the Qandil Metamorphic Series and Mawat Ophiolite Complex inside the Penjween – Walash Zone.

PETROLOGY OF HOST ROCKS AND COPPER MINERALIZATION

- **Mawat District**

– **Host rocks:** Metabasalt, metagabbro, serpentinized peridotite and quartz veins are the main host rocks of copper mineralization in the Mawat ophiolite (Hadi *et al*., 2010; Yassin *et al*., 2015). Fine clinopyroxene (50% vol.) and plagioclase (35% vol.) represent the major mineral phases of the metabasalt. Amphibole and chlorite are the alteration products of clinopyroxene. Plagioclase is characterized by deformation lamellae and partially altered into epidote (Fig.3A and B). Amphibole shows zonation of white amphibole in the core to green amphibole at the rim (Fig.3C). Porphyritic texture is dominated by clinopyroxene and plagioclase phenocrysts. Amygdales filled with secondary quartz with wavy extinction and sutured boundary and poikilitic texture are also observed.

Amphibole is the common mineral, present in white and green colors. The most abundant is the white amphibole (tremolite-actinolite) overprinting preexisting pyroxene (Fig.3D). Opaque minerals are enclosed in green amphibole and form poikiloblastic textures (Fig.3E). Late fibrous amphibole is overprinting texture of an early plagioclase. The fibrous amphibole appears to have formed during a second metamorphic episode accompanied by deformation (Fig.3F). Most of the primary plagioclase is altered to secondary minerals due to metamorphism and deformation. Epidote is the most common secondary mineral with fine grained massive form (Fig.3G). Fine grains of plagioclase formed along grain boundary and fractures by recrystallization (Fig.3H). Secondary quartz is characterized by lenticular shape, andulose extinction and deformation bands (Fig.4A). Chlorite is an abundant mineral and shows schistosity texture in metagabbro and metabasalt (Fig.4B).

– **Ore minerals:** Sulfides and oxides are the only ore minerals found in the metabasalt, metagabbro and quartz veins. They mostly exist in the form of disseminated, small aggregates and veinlets. The primary mineralogy is rather simple; sulfides are dominated by pyrite as the major sulfide mineral in addition to minor amounts of chalcopyrite. Two pyrite generations are recognized: Pre-tectonic pyrite and Post-tectonic pyrite (Yassin *et al*., 2015 and Yara and

Mohamad, 2018). Pyrite with brecciation texture and weak anisotropy of isotropic elements represents the pre-tectonic type (Ramdohr, 1980; Craig and Voughan, 1981; Awadh, 2006, Fig.4C). This type was probably deformed during regional tectonic events of the Eurasian and Arabian plates obduction and subduction. It is characterized by brecciation and cataclastic texture (Fig.4D) and rim and vein replacement texture by hematite and goethite (Fig.4E) (Yara andMohammad, 2018). On the other hand, the idiomorphic pyrite represents post-tectonic pyrite formed after the tectonic events (Fig.4F) (Musa 2007, Yassin *et al*., 2015 and Yara and Mohammad 2018).

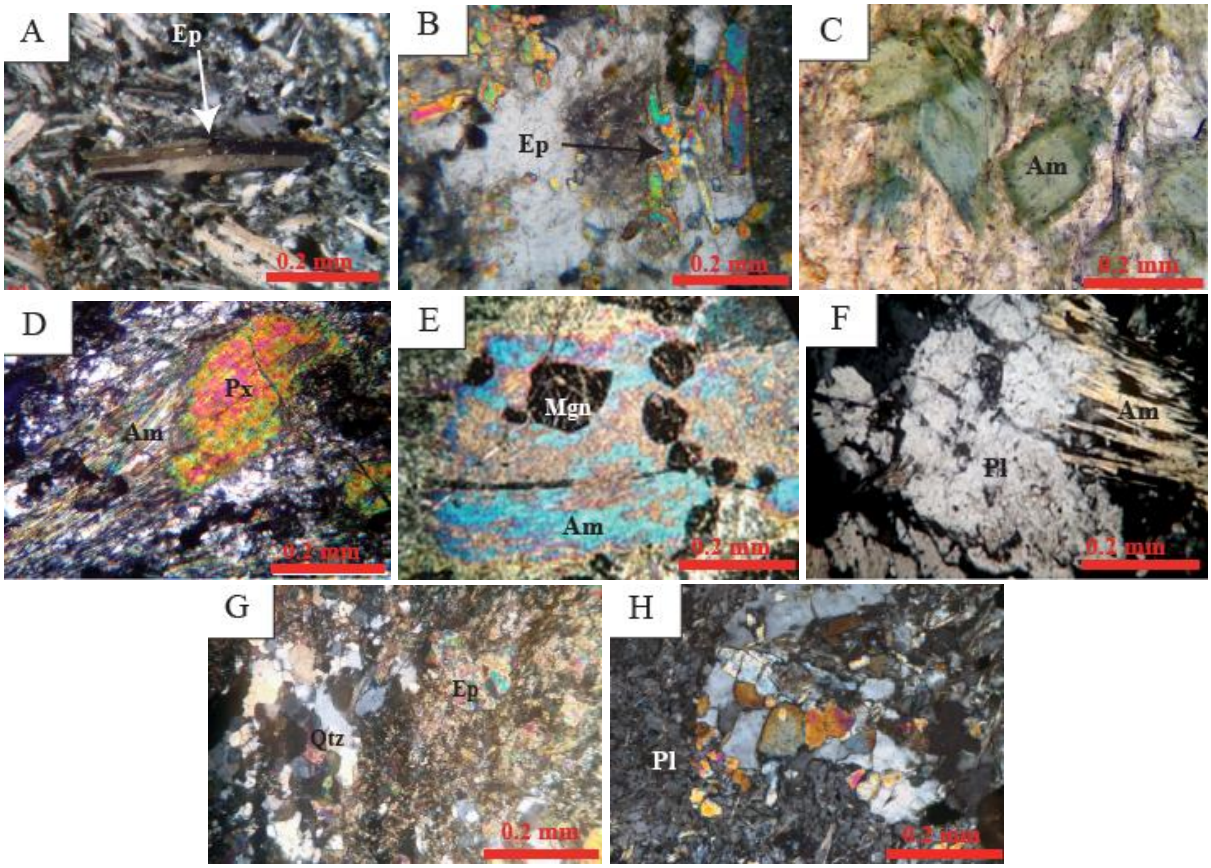

Fig.3: Photomicrographs showing **A)** Plagioclase (Pl) crystals bent due to deformation, **B)** Plagioclase is altered to epidote (Ep) in the core, **C)** Zonation in amphibole (Am), **D)** Pyroxene (Px) altered to amphibole along their edge, **E)** Poikiloblastic textures of less fibrous amphibole enclosed magnetite (Mgn), **F)** Fibrous amphibole penetrating into adjacent plagioclase crystals, **G)** Plagioclase altered to massive epidote, **H)** Plagioclase show recrystallization to fine grained. Under the microscope the major mineral phases in metagabbro are pyroxene, amphibole, chlorite, magnetite, epidote, plagioclase and quartz. (After Hadi *et al*., 2010 and Yara and Mohammad, 2018)

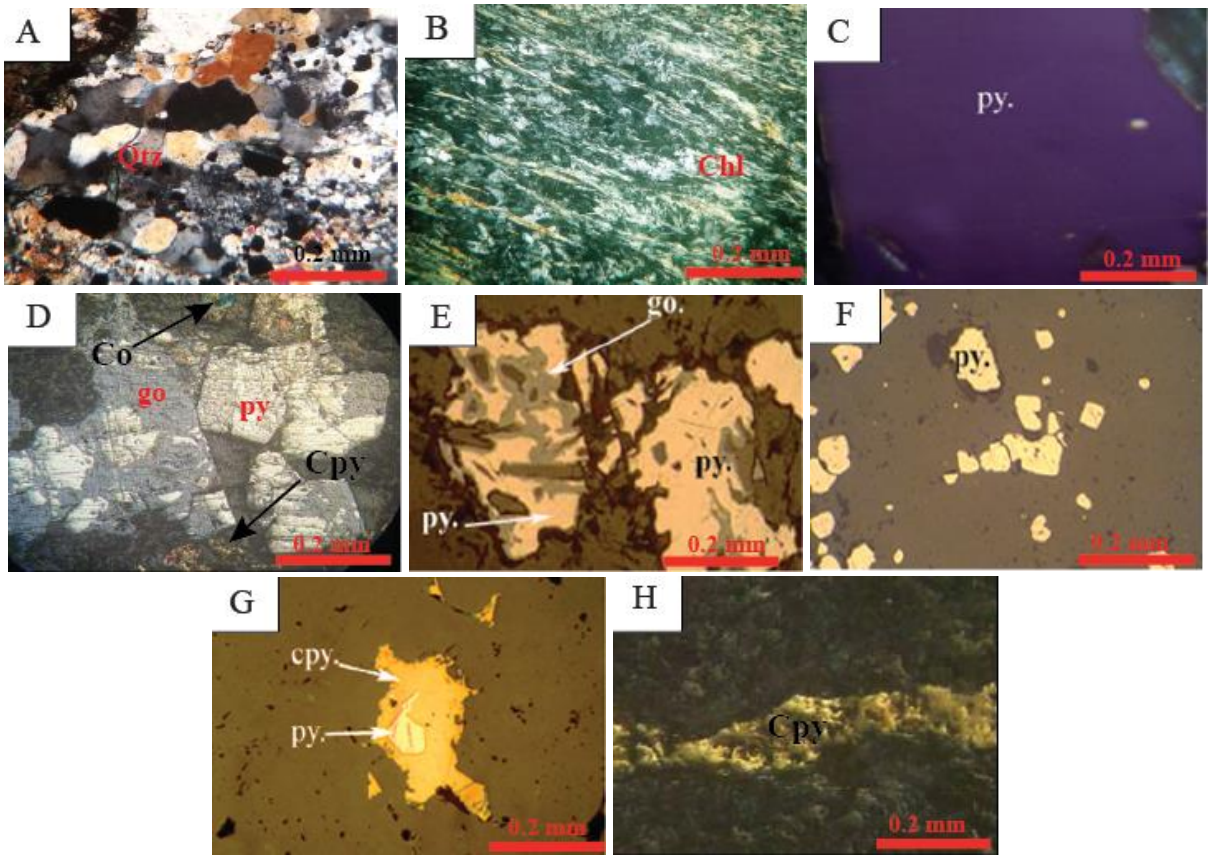

Fig.4: Photomicrographs showing **A)** Lenticular quartz (Qtz) with andulose extinction, **B)** Chlorite (Chl) showing schistosity, **C)** Pyrite grain (Py) shows weak anisotropy, observed as dark blue color, **D)** Cataclastic texture of pyrite and the goethitziation of pyrite, **E)** Rim zone replacement texture of pyrite by goethite (Go), **F)** Fine grain idiomorphic pyrite, **G)** Poikilitic texture, small grains of pyrite trapped into chalcopyrite (Cpy), **H)** Vein of chalcopyrite, after etching by HNO3 (After Musa, 2007, Yassin *et al*., 2015 and Yara and Mohammad, 2018)

Chalcopyrite is the only copper-bearing primary mineral and it is characterized by irregular form scattered in the rocks as disseminated (Fig.4G) or as veinlets filling (Fig.5H) (Musa, 2007 and Yassin *et al*., 2015). The former texture indicates that the sulfide minerals were derived from immiscible sulfide liquids (Ramdohr, 1981), whereas the latter texture indicates the hypogene origin of the ore minerals (Lufkin, 2010). Chalcopyrite is often replaced by various types of secondary minerals due to alteration and metamorphism (Musa, 2007; Yassin *et al*., 2015 and Yara and Mohammad, 2018). The most common type is rim replacement by secondary sulfides (covellite and bornite, Figs.5A and 5B respectively) and iron hydroxide (goethite and hematite, Figs.5C and 5D respectively). Malachite and azurite show zonal texture (Fig.5E) developed from the progressive intermittent replacement of chalcopyrite by oxidizing solutions. Chalcocite replaces chalcopyrite forming core replacement texture (Fig.5F). Vein replacement due to alteration is also observed between chalcopyrite with covellite (Yassin *et al*., 2015). Ilmenite and magnetite are the primary oxide minerals. They are observed forming exsolution texture (Fig.5G), while goethite and hematite are replacing the primary oxides forming rim and vein replacement texture (Fig.5H).

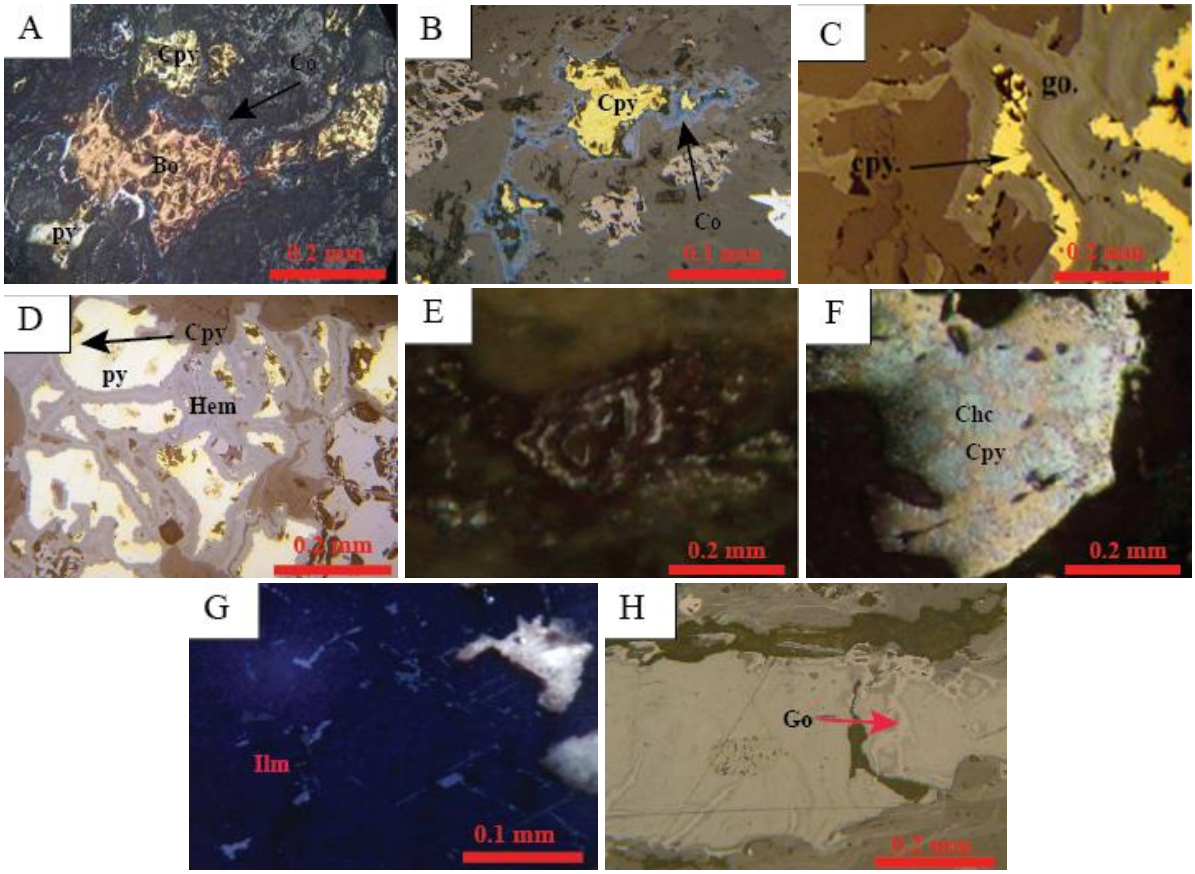

Fig.5: Photomicrographs showing **A)** Bornite (Bo) replaces chalcopyrite (Cpy) and pyrite (Py) surrounded by covellite, **B)** Covellite (Co) forming rim-replacement texture, **C)** Veinreplacement texture of chalcopyrite by goethite (Go), **D)** Chalcopyrite forming islands arc replacement, **E)** Zoning texture after etching by HNO3, **F)** Atoll texture, after etching by HNO3, between chalcocite (Chc) and chalcopyrite, **G)** Exsolution between magnetite and ilmenite (Ilm), **H)** Vein replacement of goethite (After Musa, 2007; Yassin *et al*., 2015 and Yara and Mohammad, 2018)

- **Qandil District**

– **Host rocks:** The copper mineralization is hosted by quartz veins within marble and phyllite of the Qandil Series at the Sharosh area (Mirza *et al*., 2017 and Mirza and Rashid, 2018). Phyllite and marble at Sharosh area are found as lenticular massive bodies/beds usually fractured and less often brecciated with wide spread quartz veins and veinlets that cut across both rock units. Petrographic study of ten thin sections and XRD data show that the main mineral phases of the marbles is calcite, dolomite, quartz, sulphides and traces of malachite (Fig.6). Calcite characterized by deformation twin (Fig.7A) due to regional metamorphism (Barker, 2014). Subhedral to anhedral quartz phenocrysts grains found as disseminated in marble with serrated boundaries, and undulose extinction (Fig.7B). In addition, muscovite grains occur as mica fish, mostly near the contact to the quartz veins (Fig.7C) (Mirza *et al*., 2017). Phyllite shows a poorly foliated texture under microscope and the main mineral assemblage consists of quartz, calcite chlorite and dark green amphibole, with a minor constituent of Fe-oxides (Fig.7d). In addition, X-ray diffraction data revealed the presence of illite-dominated mixed clay layers and Fe chamosite (Mirza *et al*., 2017).

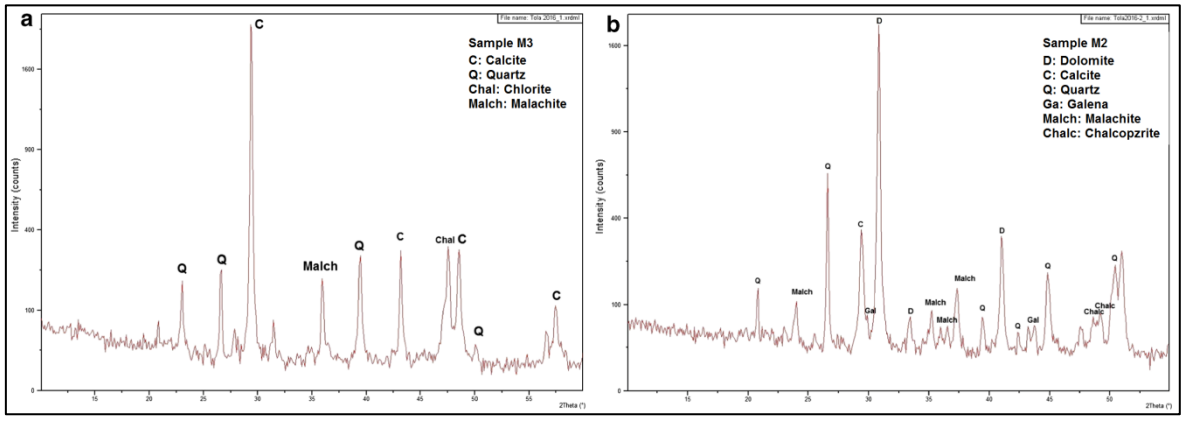

Fig.6: X-ray diffractograms of host rocks: **a)** Calcitic marble, **b)** Dolomitic marble (after Mirza *et al*., 2017)

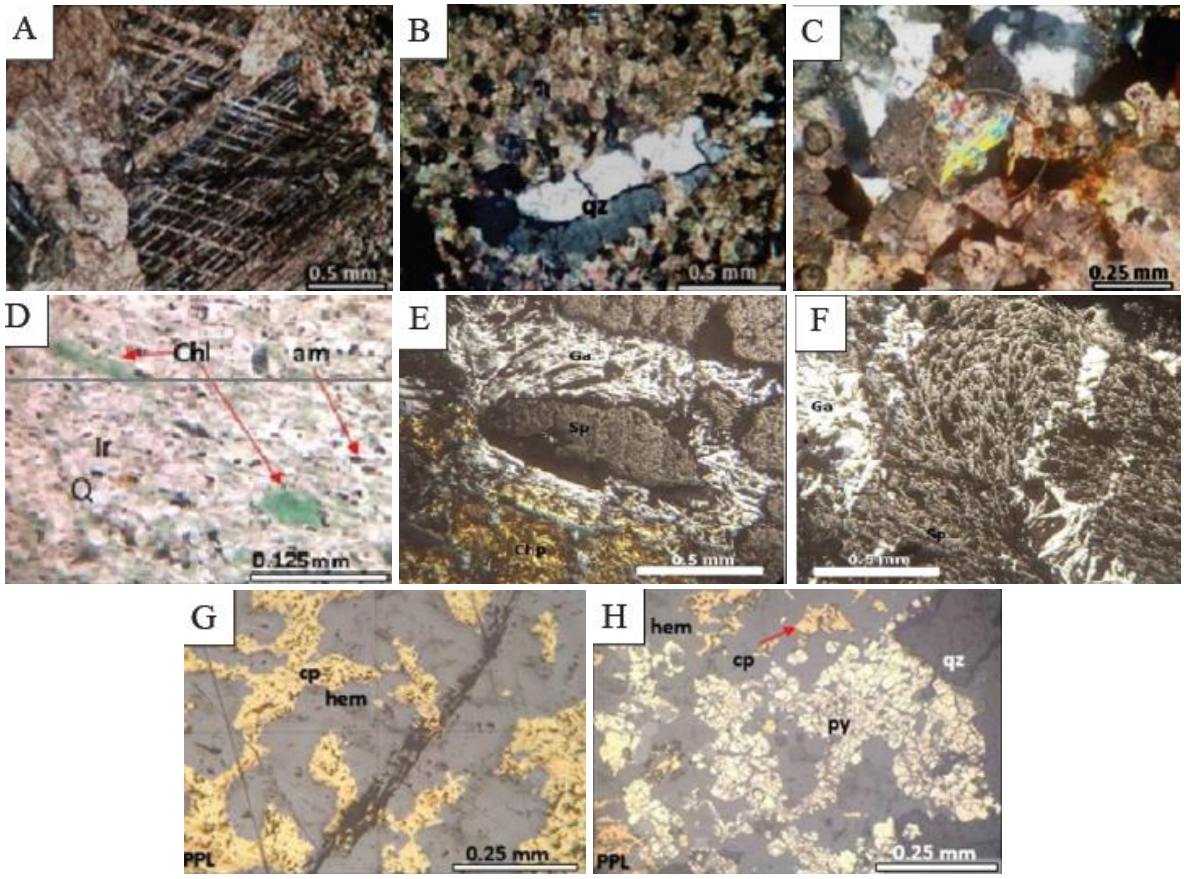

Fig.7: Photomicrographs showing: **A)** Deformation twin in calcite placed in the extinction position, **B)** Elongated quartz in calcite matrix showing simple twining, **C)** Grain of muscovite (mu) as mica fish, **D)** Phyllite showing fine-grained groundmass with quartz (Q), calcite (C), chlorite (Ch), amphibole (am) and Fe oxides (Ir), **E)** Mineralized vein containing sphalerite (sp) chalcopyrite (chp) and galena (Ga); sphalerite and chalcopyrite are replaced by rimmed galena forming augen texture, **F)** Ore vein comprising galena and sphalerite assemblage, with sphalerite replacing chalcopyrite and galena, **G)** Chalcopyrite (cp) replaced by hematite (hem), **H)** Brecciation texture of pyrite (py) (after Mirza *et al*., 2017)

– **Ore Minerals:** Subhedral and anhedral granular textures are the most abundant textures observed in the Cu ore minerals of quartz veins at Sharosh area, formed as a result of different degrees of crystallization. The primary minerals were replaced by other minerals during hydrothermal activity, forming replacement and remnant replacement textures. Chalcopyrite and pyrite were replaced by hematite and sphalerite was replaced by iron oxide (Figs.7E – H and Fig.8A and B). Secondary minerals, like malachite, azurite, goethite, hematite, tenorite and covellite, are generated from the alteration of chalcopyrite and pyrite (Figs.8C – E). Interlocking texture is observed between hematite and chalcopyrite and arranged in alignment with the host rock fabric and parallel to the trend of the shear zone (Fig.8f). Galena mostly appears as deformed micro-veins showing bands and characteristic triangular pits (Fig.8G) (Mirza *et al*., 2017).

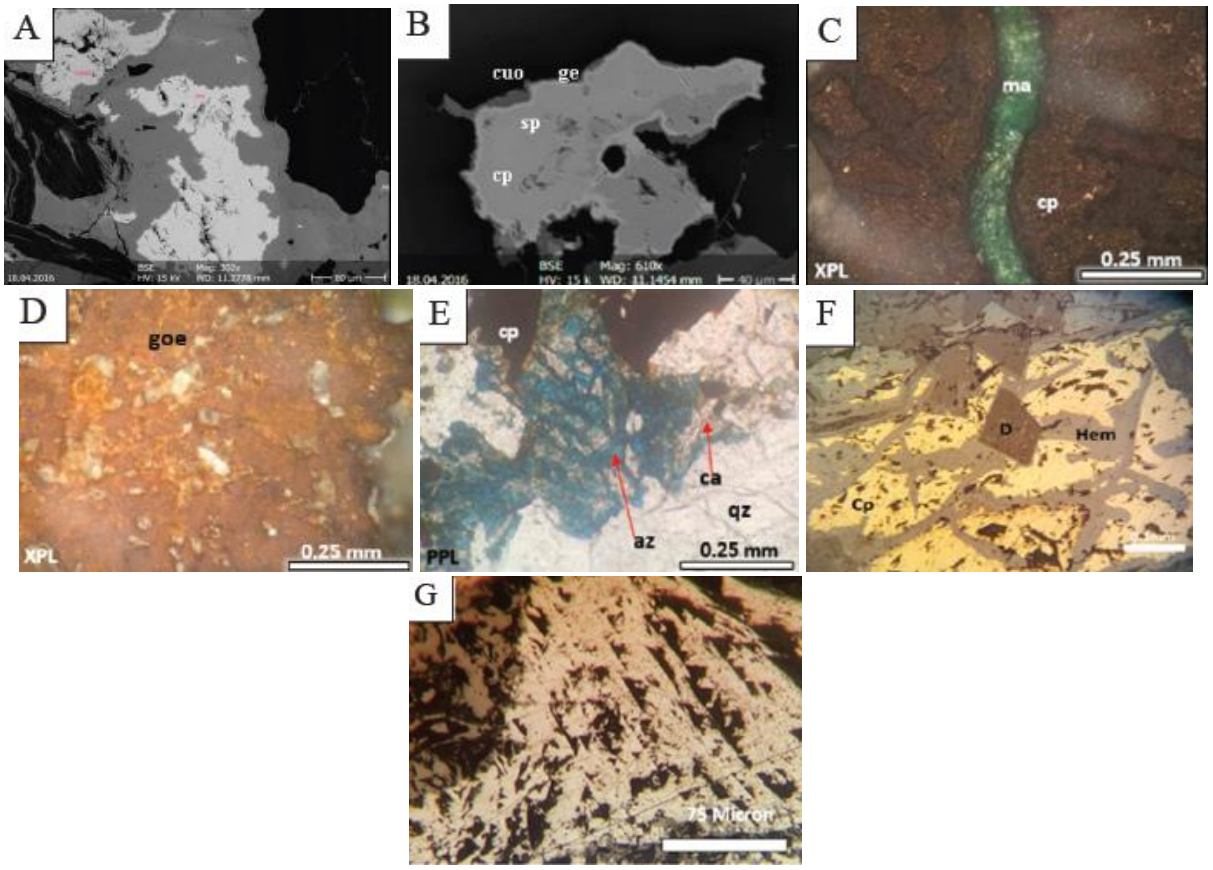

Fig.8: **A)** Back-scattered image shows sphalerite (sp) grain replaced by iron oxide, **B)** Backscattered image shows replacement of sphalerite and chalcopyrite by tenorite (te) and geerite (ge), **C)** Photomicrograph of malachite (ma) shows vein replacement texture in chalcopyrite (cp), **D)** Photomicrograph of goethite (goe) shows red-brown internal reflection, **E)** Photomicrograph of azurite (az) shows vein filling texture around dissolved carbonate veins, **F)** Photomicrograph of interlacing texture between hematite, chalcopyrite and rhombohedral dolomite (D) of the host rock, **G)** Photomicrograph of deformed galena showing bands and characteristic triangular pits (after Mirza *et al*., 2017)

GEOCHEMISTRY

The results of 28 whole rock geochemical analyses are listed in Tables 1, 2 and 3. The data from Musa (2007), Hadi *et al.* (2010) and Mirza *et al*. (2017) are used to illustrate the compositional characteristics of host rocks from the Mawat ophiolites and the Sharosh area.

Table 1: Concentration of major elements (in wt.%), trace and rare earth elements (in ppm) of the Waraz samples, Mawat area (after Musa 2007)

	W0	W1	W16	W31	W55	W57	W9	WBH-1	W12	W69
SiO_2	50.63	43.62	42.92	54.50	54.37	53.96	51.75	49.41	39.59	41.23
Al_2O_3	14.21	9.88	15.12	11.37	13.16	14.52	13.81	15.54	17.61	18.35
Fe_2O_3	8.91	7.63	13.72	9.01	7.88	10.06	9.01	15.47	15.60	16.22
CaO	10.07	18.04	19.42	10.79	10.32	7.15	8.16	2.50	19.82	16.78
MgO	9.78	8.90	6.53	9.76	10.58	5.07	10.49	7.53	3.38	0.58
Na_2O	3.47	2.52	0.24	1.87	2.11	4.24	3.75	2.99	0.32	0.04
K_2O	0.23	0.14	0.02	0.10	0.09	0.14	0.17	0.11	0.03	0.00
Cr_2O_3	0.171	0.160	0.115	0.057	0.116	0.015	0.114	0.012	0.082	0.012
TiO2	0.28	0.20	0.34	0.22	0.23	0.64	0.37	0.55	0.41	0.69
MnO	0.127	0.473	0.332	0.165	0.129	0.202	0.168	0.268	0.223	0.206
P_2O_5	0.02	0.04	0.04	0.02	0.03	0.02	0.01	0.04	0.03	0.05
LOI	1.49	8.07	1.89	1.36	2.48	2.56	1.98	5.24	2.59	4.75
Total	99.92	99.68	100.69	99.22	101.51	98.56	99.79	99.66	99.67	98.89
Trace ppm										
Sc	44	37	31	45	40	40	47	38	35	39
Ag	<.5	<.5	0.8	<.5	<.5	<.5	<.5	<.5	8.5	0.8
Ba	45.0	98.2	1.5	12.5	18.7	14.7	36.9	8.1	1.7	1.1
Ce	2.4	1.2	2.9	0.8	0.8	2.5	1.4	2.5	2.5	2.5
Co	13	6	10	7	12	14	26	28	29	30
Cr	1170	1094	787	390	793	103	780	82	561	82
Cu	14	25	1353	43	62	57	621	179	12565	1106
Dy	1.5	1.0	1.7	1.1	1.0	1.9	1.4	2.0	1.8	2.2
Er	1.2	1.0	1.2	0.9	0.7	1.4	0.9	1.5	1.3	1.6
Eu	0.2	0.2	0.4	<0.1	0.2	0.4	0.4	0.4	0.5	0.8
Ga	9.3	7.2	26.2	8.3	8.8	13.7	10.4	14.5	29.8	31.9
Gd	1.0	0.7	1.3	0.6	0.6	1.3	0.9	1.5	1.3	1.4
Ho	0.4	0.3	0.4	0.3	0.2	0.4	0.3	0.5	0.4	0.5
La	1.1	0.7	1.8	0.0	0.0	0.7	0.0	0.8	1.1	0.8
Lu	0.2	0.2	0.2	0.2	0.1	0.2	0.2	0.3	0.2	0.3
Nd	1.2	1.1	2.7	0.8	0.8	2.3	1.5	2.3	2.4	2.4
Ni	77	34	30	12	53	11	57	33	46	5
Pr	0.2	0.2	0.5	0.1	0.1	0.4	0.3	0.5	0.4	0.5
Rb	5.2	2.1	0.1	1.2	0.6	1.0	2.3	1.5	0.0	0.0
Sm	0.6	0.4	1.0	0.4	0.5	0.9	0.7	1.0	1.0	1.1
Sr	115.8	87.0	129.8	52.0	75.7	104.8	100.8	52.9	178.5	819.9
Tm	0.2	0.1	0.2	0.1	0.1	0.2	0.2	0.3	0.2	0.3
U	0.0	0.1	0.7	0.0	0.0	0.1	0.0	0.4	0.1	0.2
V	236	170	417	220	190	293	215	251	391	403
W	1.2	0.5	1.8	1.5	1.1	3.0	0.8	1.6	2.9	4.1
Y	11.1	8.6	12.1	7.1	6.5	12.1	7.5	13.8	13.1	15.0
Yb	1.3	1.1	1.5	0.9	1.0	1.5	1.1	1.8	1.5	1.9
Zn	18	9	12	11	16	66	27	119	58	15
Zr	8.2	4.6	17.3	5.2	4.7	18.5	10.3	19.4	16.0	22.5

Table 2: Major and trace elements composition of the Sharosh marble host-rock (after Mirza *et al*., 2017)

Oxide	M1	M2	M3	M4	M5	M6	M7	M8	M9	M10
SiO_2	13.82	16.32	16.70	15.20	10.48	15.20	15.19	10.06	14.76	11.98
TiO_2	1.64	0.18	0.27	0.13	0.08	0.13	0.04	0.07	0.09	0.11
Al_2O_3	3.02	4.86	4.68	3.72	2.02	4.72	0.91	3.57	3.87	4.93
Fe_2O_3	2.48	12.47	2.12	12.39	7.85	10.39	9.77	10.68	12.12	11.70
MnO	0.15	0.22	0.03	0.05	0.08	0.05	0.19	0.28	0.27	0.24
MgO	0.73	16.22	0.58	17.68	18.77	17.28	15.53	17.08	17.82	18.82
CaO	76.85	42.95	73.64	47.12	55.71	47.15	53.70	52.84	46.23	50.37
Na_2O	0.37	0.22	0.11	0.04	0.38	0.04	0.04	0.05	0.03	0.07
K_2O	0.85	1.18	1.36	0.57	0.37	0.56	0.22	0.37	0.47	0.48
P_2O_5	0.06	0.08	0.06	0.03	0.03	0.05	0.02	0.02	0.03	0.03
SO_3	0.01	2.48	0.05	2.03	3.40	3.45	3.51	3.67	3.52	3.99
Cl	0.01	0.01	0.01	0.03	0.05	0.03	0.04	0.02	0.04	0.03
Sum	100.0	97.2	99.6	99.0	99.2	99.1	99.2	98.7	99.3	98.8
Trace ppm										
Ni	83.1	236.2	72.4	13.1	24.0	13.2	273.0	21.9	21.6	24.9
Rb	56.3	68.6	79.2	24.0	12.3	25.0	8.8	14.9	17.6	21.1
Sr	2095.5	371.7	1618.6	508.0	845.0	506.0	142.0	198.0	85.4	106.5
Cu	105.3	22,940.0	1850.0	1145.3	1166.0	1345.3	10,021.0	1590.0	856.0	711.0
Co	72.5	159.4	126.6	5.7	4.0	5.0	51.9	26.1	17.2	16.0
W	350.5	218.3	829.3	31.0	4.5	31.0	65.0	93.3	8.7	3.5
Zn	0.0	3579.1	0.0	1122.0	1126.0	1022.0	936.0	86.0	123.0	1051.0
Zr	45.0	82.5	124.0	12.6	11.1	11.6	7.3	12.4	15.3	14.9
As	<d.l.	49.8	<d.l.	6.3	2.6	8.6	82.2	335.5	43.5	35.0
Ba	<d.l.	533.5	317.9	50.0	60.0	49.3	110.0	190.0	190.0	190.0
Ce	<d.l.	<d.l.	<d.l.	<d.l.	<d.l.	<d.l.	<d.l.	<d.l.	<d.l.	<d.l.
Ga	<d.l.	<d.l.	<d.l.	3.6	2.4	9.8	<d.l.	<d.l.	<d.l.	5.7
Y	<d.l.	<d.l.	<d.l.	11.8	10.1	<d.l.	4.6	<d.l.	8.4	<d.l.
Sum trace in ppm	2808.2	30,039.1	4018.0	2933.4	3268.0	3026.7	11,702.5	2568.1	1386.7	2179.6
Sum trace in %	0.3	3.0	0.4	0.3	0.3	0.3	0.1	0.3	0.1	0.2
Sum major and trace	100.3	100.0	100.0	99.3	99.6	99.4	99.3	99.0	99.4	99.0

Table 3: Major and trace elements composition of the Sharosh phyllite host-rocks (after Mirza *et al*., 2017)

Oxide	Ph1	Ph2	Ph3	Ph4	Ph5	Ph6	Ph7
SiO_2	49.11	48.77	55.41	61.4	77.66	64.79	59.23
TiO_2	0.72	0.87	0.65	0.63	0.47	0.84	0.56
Al_2O_3	15.35	13.55	13.17	16.89	8.22	14.66	12.98
Fe_2O_3	9.00	10.30	5.11	5.89	3.77	4.99	4.86
MnO	0.11	0.14	0.08	0.1	0.04	0.29	1.83
MgO	3.91	3.27	3.1	1.99	1.24	2.31	4.02
CaO	16.94	17.45	16.21	7.39	5.4	6.69	10.11
Na_2O	1.22	1.42	1.28	0.32	1.08	0.99	1.3
K_2O	3.10	3.56	2.78	3.71	1.49	2.88	2.68
P_2O_5	0.19	0.09	0.16	0.16	0.09	0.09	0.15
SO_3	0.01	0.02	0.01	0.02	0.02	0.14	0.2
Cl			0	0.1	0	0.09	0.085
Sum	99.66	99.44	97.96	98.6	99.48	99.76	98.005
Trace ppm							
Ni	143.40	98.00	49.1	66.8	29.9	56.9	48.67
Rb	135.10	140.40	74.4	152	58.5	114	89.78
Sr	448.50	456.32	185.5	133	43.5	45.66	56.98
Cu	251.70	345.00	93.3	52.4	11.5	101.45	88.32
Co	116.50	109.98	14.8	20.2	9.5	15.87	21.12
W	449.40	488.57	2.5	1820	5.5	423.11	136.43
Zn	146.10	139.89	76	86	49	75.34	35.6
Zr	247.50	239.58	25.1	23.4	37.1	39.11	20.1
As	<d.l.	25.10	9.2	31.5	2.1	32.24	31.22
Ba	889.90	768.47	380	370	270	400.01	602.34
Ce	<d.l.	400.00	211	365.35	268.12	<d.l.	111.03
Ga	33.68	26.70	18.55	24.2	10.2	22	30.11
Y	30.36	31.12	13.5	10.7	7.1	8.9	9.94
Sum trace in ppm	2892.14	3269.13	1152.95	3155.55	905.52	1334.59	1281.64
Sum trace in %	0.30	0.33	0.12	0.32	0.01	0.13	0.13
Sum major and trace	99.96	99.77	98.08	98.92	99.49	99.89	98.14
SiO_2/Al_2O_3	3.2	3.60	4.21	3.64	9.45	4.49	4.56
K_2O/Na_2O	2.54	2.51	2.17	11.59	1.38	2.91	2.06
K_2O/Al_2O_3	0.202	0.26	0.21	0.22	0.18	0.20	0.21

- **Geochemistry of Country Rocks**

– **Metagabbro and metabasalt of the Mawat Ophiolite Complex in the Waraz area:** The samples from the Waraz area exhibit a wide range of SiO2 content (39.59 – 54.5 %, Table 1), indicating magmatic fractionation and alteration (Shafaii *et al*., 2010). Generally the samples are characterized by low TiO2 (0.2 wt.% – 0.69 wt.%), low Zr (4 – 22 ppm) and high Mg# (49 – 1273), showing boninitic affinity (Crawford *et al*., 1989). Most of the samples show depletion of high field strength elements (HFSE) with low Zr/Y ratio (Table 1) referring to depleted mantle source (Pearce and Norry, 1979). A wide range in Cu content (14 – 12565 ppm) is observed showing a negative correlation with MgO, Co and Ni which may be attributed to segregation of immiscible melt (Scoates and Mitchel, 2000).

On the spider diagram (Fig.9) the large ion lithophile elements (LILE) and the HFSE have depleted values and they lie parallel but at lower level than those of the mid-oceanic ridge basalts (MORB) values which may be indicating oceanic island arc tholeiitic basalt or reflecting the pre-subduction characteristic of the source mantle (Miyashiro and Shido, 1975; Wilson, 1989; Xu *et al*., 2003; and Maheo *et al*., 2004). The diagram in Fig. (9) shows enrichment of some LILE relative to other elements. The concentrations of these elements may be affected by hydrothermal alteration processes and hence reflect involvement of these elements to the source melt during the subduction process (Hadi *et al*., 2010).

The REE patterns are characterized by a slight depletion in the light rare earth elements (LREE) relative to the heavy rare earth elements (HREE) where (LaN/SmN = 0.49 – 1.29) (Fig.10). The negative Eu anomaly (Eu/Eu* = 0.89) for the basalt samples W0, W9 and WBH-1 can be attributed to the cumulative effects of plagioclase fractionation (Van Wagoner *et al*., 2002; Zhang *et al*., 2003), while the positive Eu anomalies (Eu/Eu*)ave = 1.25 for the other analysed rock types can be attributed to model concentration of plagioclase in the rocks and accumulation of calcic plagioclase which influences the increase of Eu^{2+} (Al-Hassan, 1987; Savov *et al*., 2001). According to the Ti/V ratio (4.8 – 10.2), the samples lie in the region of island arc tholeiite and boninite field of Shervais (1982) (Fig.11). Such behavior is characteristic of back-arc basin basalt (Pe-Piper *et al*., 2004). The very low concentration of the REE and enrichment of the HFSE and LILE indicate that these rocks were derived from a depleted mantle source (Hadi *et al*., 2010).

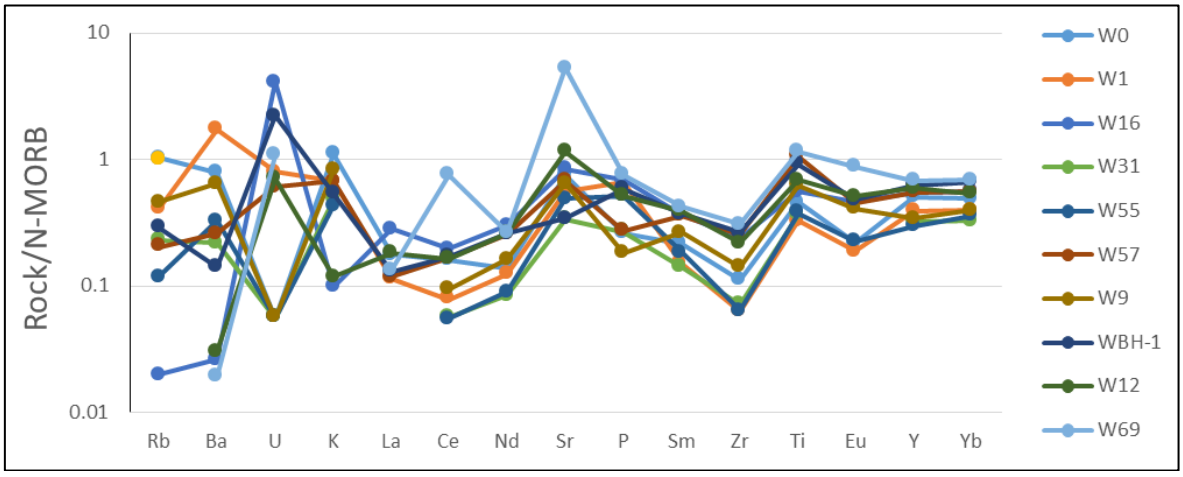

Fig.9: Spider diagram of Waraz host rocks (after Hadi *et al*., 2010) normalized according to the values of Sun and McDonough (1989)

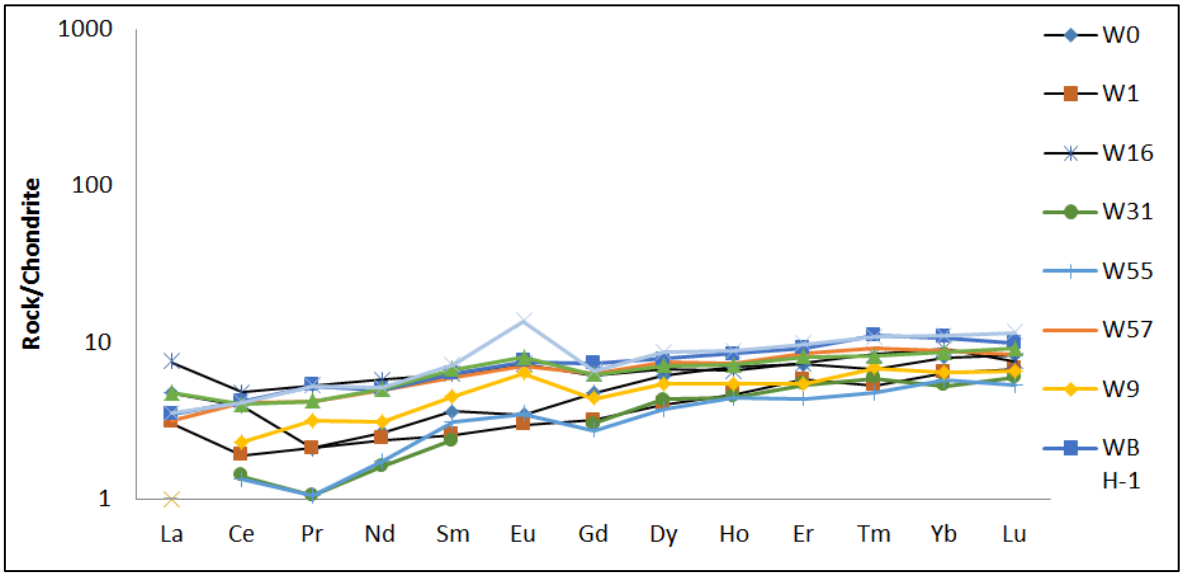

Fig.10: Chondrites-normalized REE pattern of the mafic rocks of Waraz (after Hadi *et al*., 2010). Normalization values are after Sun and McDonough (1989)

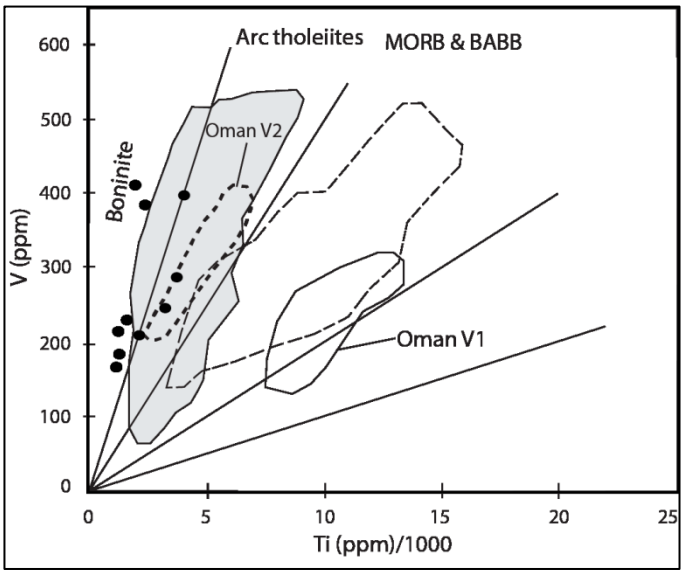

Fig.11: Ti versus V diagram (Shervais, 1982) for Waraz mafic rocks (black circles) (after Hadi *et al*., 2010)

– **Marble and Phyllite:** Two types of marble have been distinguished in the Sharosh area: the first one is calcite marble and contains <1% MgO (Samples M1 and M3), whereas the second type is dolomitic marble (MgO = 15.53% – 18.82%) (Table 2, Mirza *et al*., 2017). The SiO_2 abundance in the marble covers a range (10.48% – 16.70 %), related to quartz and indicating deposition in shallow depth of protolith and increased terrestrial influx. The marble samples are characterized by very low total alkalis ($Na_2O + K_2O < 2\%$). The abundance of silicate minerals in the dolomitic marble samples shows relatively higher values of K_2O and Al_2O_3. The marble was affected by hydrothermal alteration, emphasized by the poor correlation between Ba, Sr and Zr. The Sharosh phyllites are characterized by moderate SiO_2 and Fe_2O_3 contents ranging between 48.77 and 77.66 wt.% and 3.77 to 10.30 wt.%,

respectively (Table 3). Figure (12) shows the different types of rocks. Based on the Fe_2O_3/K_2O vs. SiO_2/Al_2O_3 ratios, the analysed Sharosh phyllite samples lie in the wacke and lithic arenite fields (Herron, 1988).

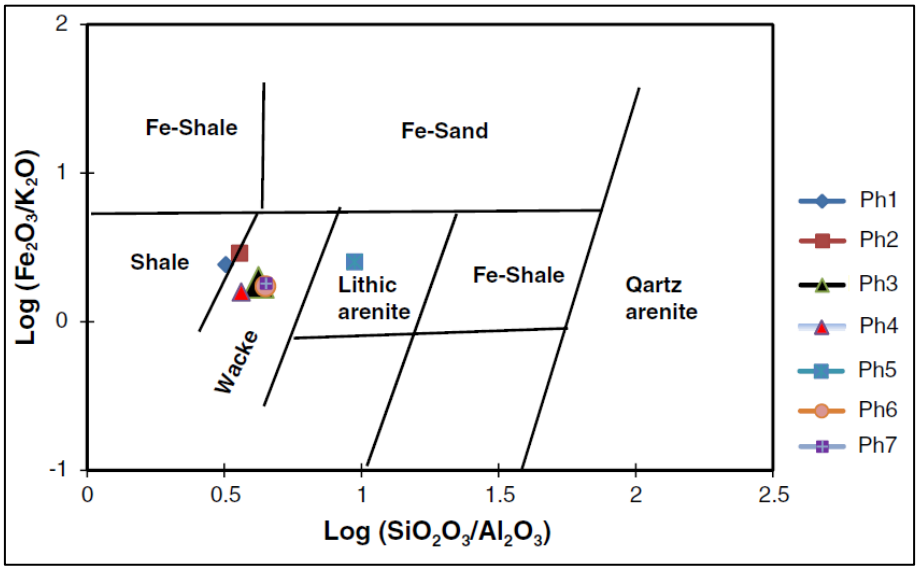

Fig.12: Geochemical classification of the Sharosh phyllites
(after Herron, 1988)

- **Geochemistry of Sulfide Minerals**

The bulk sulfide veins of the Sharosh mineralization have high Cu content (0.2% – 33.2%) and CaO content (0.66% – 24%) (Table 4). The origin of the sulfides can be assessed by Ti vs. Ni/Cr and Cr vs. V diagrams of Dare *et al*. (2014) which indicate that all samples of this study lie in the hydrothermal field as shown in Figure (13).

- **Fluid Inclusions**

Primary and liquid-rich type of fluid inclusions have been recognized in the quartz associated with copper mineralization in the Qala Diza area (Qandil Series) by Mirza and Rashid (2018), Figs.14 and 15). Freezing-heating stages and fluid inclusion assemblages were selected based on the criteria and recommendations of Roedder (1958 and 1984); and Goldstein (2003). Salinities are expressed as wt.% NaCl equivalent and are estimated from the melting temperatures of the last crystal of ice for two-phase fluid inclusions (Bodnar, 1993). The fluid inclusions range in size between 7.2 and 19.3 µm, and 18 – 50 % of vapor/liquid/ (V/L) ratio (Mirza and Rashid, 2018). The measured eutectic temperatures range between -35 °C to -48 °C define its composition in the H_2O-KCl-$CaCl_2$-NaCl, possibly with smaller amounts of $MgCl_2$ (Fig.14a). Ice from quartz melted between -1.5 °C and 4.6 °C, corresponds to salinities of (2.6 – 7.3) wt.% NaCl eq. (Fig. 14b). The homogenization temperature of fluid inclusions occurred between (194.1 °C) and (386.8 °C) (Fig.14c). The microthermometric data show two types of fluid inclusions, one with homogenization temperature ranging between (335.5 °C) and (386.8 °C) and the other is characterized by lower homogenization temperatures ranging between (194.1 °C) and (298.5 °C) (Fig.15A). The results of homogenization temperature and salinity of fluid inclusions refer to fluid derived from a metamorphic fluid regime (Fig.15B) (Mirza and Rashid, 2018).

Table 4: Major and trace element contents of the bulk sulfide ores at Sharosh area (after Mirza *et al*., 2017)

Sample	S101	S201	S301	S401	S402	S403	S501	S502	S601	S602	Av.
Fe %	1.07	12.00	15.00	7.39	7.20	8.20	10.00	0.66	24.00	2.30	10.98
Si %	15.00	14.00	13.00	<d.l.			16.00	11.00	1.10	0.20	8.79
Pb %	1.80	2.4	0.05	0.02	0.01	<d.l.	0.20	1.30	0.01	1.40	0.60
Zn %	0.19	2.25	1.62	2.37	3.11	9.77	0.89	0.00	6.10	0.01	3.29
Cu %	1.10	13.00	13.00	30.00	33.20	13.50	13.00	0.20	25.00	1.30	17.91
Element (mg/kg)											
Ag	31.00	84.00	26.00	12.00	<d.l.	<d.l.	63.00	114.00	75.00	179.00	73.00
Al	224.00	273.00	392.00	4037.0	4625.3	5.80	481.00	236.00	474.00	<d.l.	1343.51
As	923.00	88.00	61.00	69.00	<d.l.	<d.l.	230.00	16.00	263.00	19.00	208.63
B	4.00	1.80	<d.l.	6.30	<d.l.	<d.l.	<d.l.	2.00	<d.l.	<d.l.	1.76
Ba	13.00	129.00	54.00	85.00	<d.l.	<d.l.	41.00	90.00	234.00	24.00	83.75
Be	0.04	0.09	0.10	0.40	<d.l.	<d.l.	0.08	0.06	0.20	<d.l.	0.12
Bi	545.00	20.00	4.50	2.00	0.20	0.10	3.40	686.00	21.00	573.00	231.00
Cd	23.00	10.00	6.10	11.00	20.90	81.30	6.10	28.00	29.00	25.00	30.05
Co	103.00	97.00	67.00	202.00	141.30	129.70	162.00	62.00	36.00	15.00	126.88
Cr	15.00	37.00	<d.l.	<d.l.	<0.1	<0.1	40.00	36.00	53.00	82.00	32.88
Cs	0.05	0.20	0.06	0.30	1.20	0.50	0.20	0.20	0.30	0.04	0.38
Ga	0.50	4.50	2.80	4.60	6.70	5.30	2.00	2.50	7.90	0.70	4.69
Ge	0.90	1.20	1.50	0.50	<d.l.	<d.l.	1.30	0.60	1.10	0.01	0.89
Li	0.90	1.40	1.10	6.10	<d.l.	<d.l.	1.40	1.50	1.40	0.20	1.75
Mn	81.00	203.00	14.00	695.00	957.00	1680.8	180.00	320.00	277.00	702.00	638.73
Mo	23.00	11.00	47.00	2.50	<d.l.	<d.l.	17.00	2.70	7.30	2.20	14.09
Ni	40.00	112.00	635.00	221.00	208.10	478.00	404.00	11.00	526.00	52.00	335.89
Rb	0.50	2.40	0.60	1.00	13.50	7.00	1.80	2.70	3.30	0.30	4.14
Re	0.03	0.02	0.03	0.01	<d.l.	<d.l.	0.02	0.01	0.01	<d.l.	0.02
Se	201.00	4.90	23.00	7.50	<d.l.	<d.l.	11.00	255.00	11.00	227.00	92.55
Sr	14.00	18.00	5.20	10.00	10.90	22.90	19.00	66.00	12.00	71.00	31.13
Ti	52.00	98.00	61.00	437.00	<d.l.	<d.l.	75.00	148.00	160.00	121.00	144.00
U	6.70	36.00	17.00	28.00	14.70	7.20	19.00	2.30	7.90	1.90	17.59
V	4.90	12.00	<d.l.	13.00	<0.1	<0.1	13.00	13.00	20.00	27.00	12.86
W	1054.00	571.00	471.00	124.00	<d.l.	<d.l.	1500.00	632.00	75.00	78.00	563.13
Zr	8.90	3.40	1.90	15.00	<d.l.	<d.l.	2.80	4.80	7.00	0.70	5.56
Ni/Co	0.39	1.15	9.48	1.09	1.47	3.69	2.49	0.18	14.61	3.47	4.11

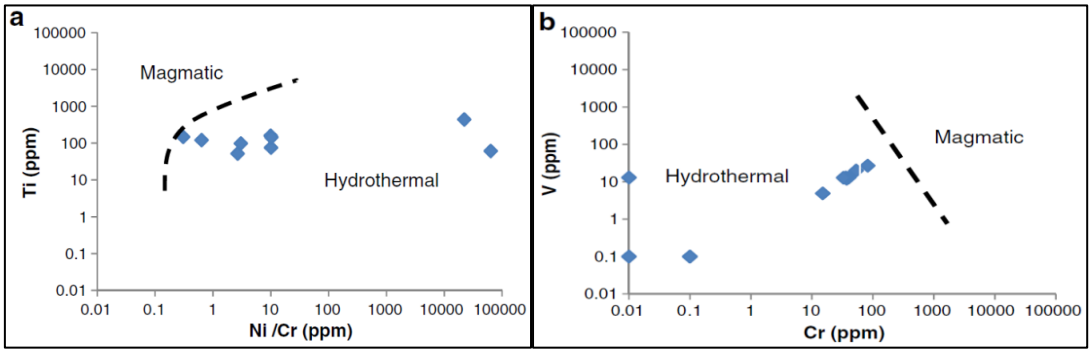

Fig.13: The Ti vs. Ni/Cr and Cr vs. V diagrams from Dare *et al*. (2014) and plots of the studied sulfide ore minerals (after Mirza *et al*., 2017). The dotted line represents the boundary between hydrothermal and igneous sulfides

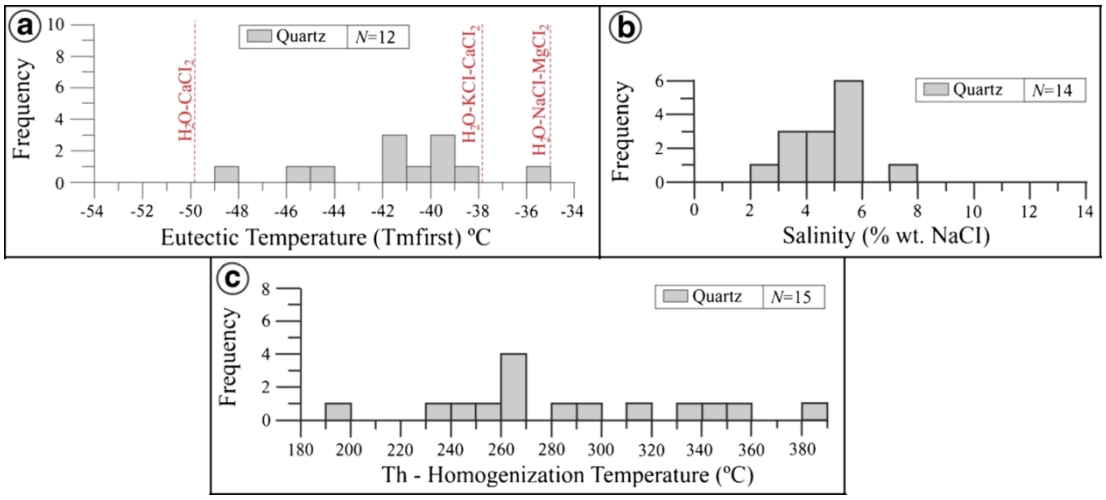

Fig.14: Frequency distributions of eutectic, salinity, and homogenization temperature of measured fluid inclusions from SH-11V sample (after Mirza and Rashid, 2018)

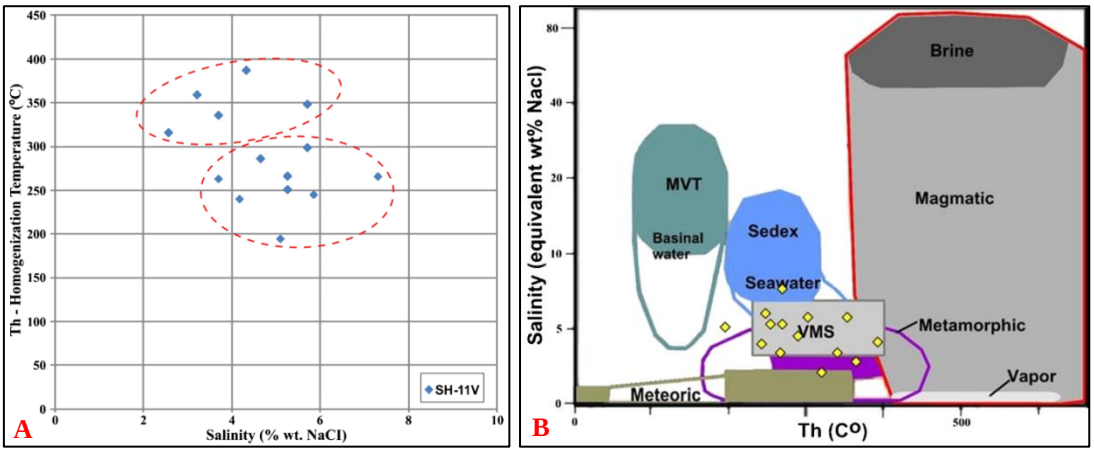

Fig.15: Fluid inclusions characteristics (after Mirza and Rashid 2018). **A)** Homogenization temperature vs. salinity (wt.% NaCl eq.) diagram of measured fluid inclusions from sample SH-11V, **B)** Determination of the ore fluid type using a homogenization temperature salinity diagram (dark zones inside lines show approximate T-salinity range for ore-forming fluids, after Kesler, 2005)

- **Sulfur Stable Isotopes**

Sulfur stable isotopes for galena and chalcopyrite have been measured in the mineralized samples of the Qala Diza area (Qandil Series) by Mirza and Rashid (2018). The galena and chalcopyrite exhibit close isotopic values of -17.7 and -17.6‰ respectively. This range is very close to the values of $\delta^{34}S$ reported by Ohmoto and Rye (1979), Nielsen (1979), Ohmoto (1986); Seal (2006) and Hoefs (2009). The $\delta^{34}S$ values of the studied sample show that the sulfur of the Sharosh sulfide minerals is in the range of sedimentary and metamorphic sources (Fig.16).

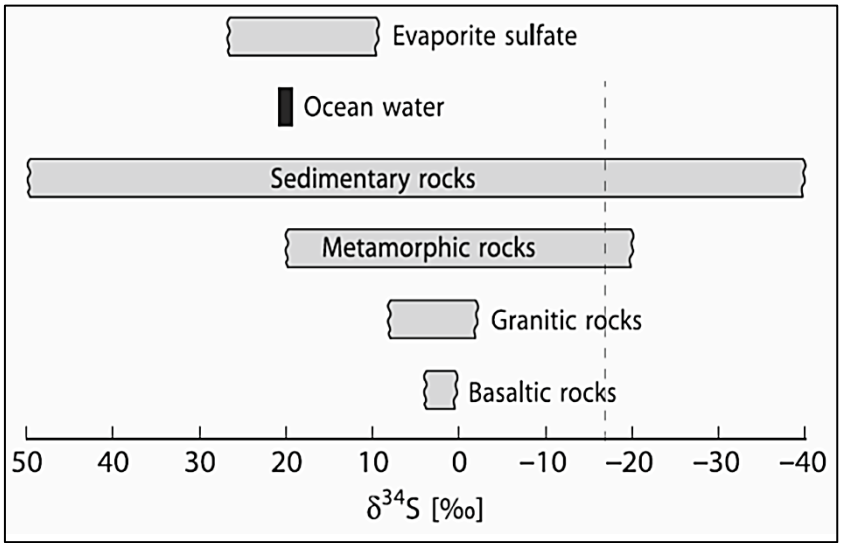

Fig.16: Sulfur isotope composition of chalcopyrite and galena from the Sharosh area (after Mirza and Rashid, 2018). The dashed line represents the sulfur isotopic composition of the analysed samples which intersects with the isotopic range of sedimentary and metamorphic sources (after Hoefs, 2009)

GENESIS

- **Mawat Ophiolite Mineralization**

The mineralogy of the copper mineralization at the Mawat Ophiolite Complex is very simple. Chalcopyrite and bornite represent the primary copper sulfides of endogenic origin. They are found as disseminations through the metagabbro and metabasalt. The origin of mineralization in the Mawat ophiolites is based essentially on petrographic and geochemical characteristics. The data show that the mineralization started in the orthomagmatic stage which formed the disseminated sulfide minerals (Hadi *et al*., 2010; and Yassin *et al*., 2015). Magmatic fluids, enriched by Fe, Ti, Cu, and volatiles through magmatic differentiation, formed immiscible sulfide liquid which was collected in the interstial space of the early-formed minerals or injected to shear zones (Pearce and Gale, 1977; and Klein and Hurlburt, 2002). This is indicated by ore microscopy observations (pyrite and chalcopyrite relation with the silicate minerals) and by geochemical data (Cr and Ni decrease as Ti increase) which indicate that the melt was enriched with Ti at the late stages of magma fractionation reaching maximum when magnetite began to crystallize (Table 1).

The replacement of the primary sulfide minerals by iron and copper sulfide minerals, forming pseudomorphic relict texture, island arc texture and rim texture, is considered to represent supergene origin (Musa, 2007; Yassin *et al*., 2015; Yara and Mohammad, 2018).

Hydrothermal solutions resulted in the copper enrichment and mineralization, forming fine euhedral pyrite and chalcopyrite filling the cavities and fractures (Hadi *et al*., 2010 and Yassin *et al*., 2015). Supergene enrichment is the last stage of mineralization where the copper mineralization underwent extensive alteration and oxidation largely by the supergene solutions. The primary sulfide minerals were altered producing secondary minerals (covellite, limonite, hematite, malachite and goethite) (Musa, 208; Hadi *et al*., 2010; and Yassin *et al*., 2015).

- **Sharosh Mineralization**

The paragenesis of copper mineralization at Sharosh area probably occurred in three stages: the first stage is represented by disseminated chalcopyrite, sphalerite and pyrite in metasedimentary rocks; the second stage is dominated by chalcopyrite, pyrite, sphalerite and galena, precipitated from metal-rich hydrothermal fluids; and the last stage is represented by supergene enrichment or alteration of preexisting minerals, dominated by hematite, goethite, malachite, azurite, geerite, covellite and tenorite (Mirza *et al*., 2017). The δ34S value refers to sulfur of hydrothermal fluid derived from the sedimentary and metamorphic country rocks such as those of the Qandil Metamorphic Series (Mirza and Rashid, 2018). Copper, Fe, Pb, and Zn were extracted from these country rocks by migration, circulation, and interaction with hydrothermal fluids, transporting them into faults and cavities which were favorable sites for ore deposition and mineralization (Mirza *et al*., 2017). The studied area is highly deformed and intersected by major and minor faults, which play a significant role for the indication and localization of the ore minerals. In addition, faults were considered to be the main conduits for the transport of ore-bearing fluids to structurally favorable sites for the deposition of ore minerals in this area (Mirza *et al*., 2017). Hypogene mineralizations, formed before the last tectonic event, are characterized by brecciation of pyrite and deformation of chalcopyrite (Fig.4) and andulose extinction, as well as bending and orientation of the muscovite crystals (Fig.2).

ECONOMIC POTENTIAL

Despite the numerous showings of copper mineralization in the Kurdistan Region of NE Iraq, none of which have been investigated in detail to enable accurate assessment of tonnage, grade, mining conditions and upgrading potential. However, in view of the numerous Cu deposits in Cyprus, Turkey, Iran and Oman, which are all related to the Cretaceous ophiolites and are commercially producing copper, it can be anticipated that the potential of discovering commercial Cu deposits in the age-equivalent ophiolite complexes of the Kurdistan Region is encouraging (Al-Bassam, 2013). This assumption is supported by the high density of Cu showings in suitable suit of host rocks in the Mawat Ophiolite Complex and in other Cretaceous basic and ultrabasic complexes in the region, as well as due to the development of subsurface supergene Cu-enrichment zone(s) in the mineralization areas. The assessment of Cu potential in the region, however, requires detailed geophysical and geochemical exploration surveys coupled with exploratory drilling in the anomalous areas. The supergene enrichment zones as well as the Cu-bearing quartz veins are potential exploration targets in this respect.

CONCLUSIONS

The copper mineralization underwent different stages of deformation and alteration, indicating that there were many mineralization periods before and after the subduction event. Two types of primary mineralization occur in the Mawat Ophiolite Complex: (1) sulfides, which are represented by pyrite and chalcopyrite, and (2) oxides, represented by magnetite

and ilmenite. The mineralization occurs as disseminated and vein filling. The mineral assemblage is chalcopyrite, pyrite, magnetite and ilmenite as primary minerals, whereas covellite, malachite, hematite and goethite are the secondary minerals. They are distributed throughout metamafic igneous rocks (gabbro and basalt) and quartz veins. The mineralization is considered as endogenic (magmatic and hypogene origin). Chalcopyrite, sphalerite, galena and pyrite as primary minerals and azurite, malachite, gerrite, tenorite covellite, and hematite as secondary minerals are the common ore mineral described in the Qandil Series, with open-space filling and replacement textures. They are distributed within metamorphic rocks (marble and phyllite. These sulfide ore minerals have been formed from mesothermal fluids. Based on field observations and evaluation of the examined samples, probably there is an economic concentration of copper that could be found under the surface of the studied areas, originated by the oxidation of covellite and the subsequent transportation of copper to a subsurface zone of second cycle enrichment.

ACKNOWLEDGMENTS

This contribution is an overview article based on research work of Iraq Geological Survey, Iraqi universities and published papers of the author and various colleagues. The author is grateful to Dr. Yousif O. Mohammad, Department of Geology, College of Science, University of Sulaimani, Iraq, for his review and insightful suggestions and comments.

REFERENCES

Alavi, M., 1994. Tectonics of the Zagros Orogenic Belt of Iran: New data and interpretations: Tectonophysics, Vol.229, p. 211 – 238.

Al-Bassam, K.S., 2007. Minerogenic map of Iraq, scale 1: 1000 000 2nd ed., GEOSERV, Baghdad, Iraq.

Al-Bassam, K.S., 2013. Mineral Resources of Kurdistan Region, Iraq. Iraqi Bul. Geol. Min., Vol.9, No.3, p. 102 – 127.

Al-Hashimi, A. R. and Al-Mehaidi, H. M. 1975. Cu-Ni-Cr dispersion in Mawat Ophiolite Complex, NE Iraq. Journal of Geological Society of Iraq, Special Issue, p. 37– 44.

Al-Hassan, M.E., 1987. Rare earth element pattern of layered gabbro of the Penjwin Complex, NE. Iraq. Ofioliti, Vol.12, p. 437 – 444.

Awadh, S.M., 2006. Mineralogy, Geochemistry and Origin of the Lead-Zinc-Barite Deposits From Selectied Areas, North of Zakho, Northern Iraq. Ph.D. Thesis, Baghdad University.

Barker, A.J., 2014. A Key for Identification of Rock-Forming Minerals in Thin Section. CRC Press, Boca Raton. 188pp.

Berberian, F. and King, G.C.P., 1981. Towards a paleogeography and tectonic evolution of Iran: Canadian Journal of Earth Sciences, Vol.18, p. 210 – 265.

Bodnar, R.J., 1993. Revised equation and table for determining the freezing point depression of H_2O – NaCl solutions. Geochim Cosmochim Acta, Vol.57, No.3, p. 683 – 684.

Campbell, I.H., Lesher, C.M., Coad, P., Franklin, J.M., Gorton, M.P. and Thurston, P.C., 1984. Rare earth elements mobility in alteration pipes below massive sulphide deposits. Chemical Geology, Vol.45, p. 181 – 202.

Craig, J.R. and Vaughan, D.J., 1981. Ore Microscopy and Ore Petrography. John Wiley and Sons. New York, 406pp.

Crawford, A.J., Falloon, T.J. and Green D.H., 1989. Classification, petrogenesis and tectonic setting of boninites. In: A.J. Crawford (ed.), Boninites and Related Rocks: London, Unwin Hyman, p. 1– 49.

Dare, S.A.S, Barnes, S-J, Beaudoin, G., Méric, J., Boutroy, E. and Potvin-Doucet, C., 2014. Trace elements in magnetite as petrogenetic indicators.Mineral. Deposita, Vol.49, No.7, p. 785 – 796.

Glennie, K.W., 2000. Cretaceous tectonic evolution of Arabia's eastern plate margin: A tale of two oceans. SEPM (Society for Sedimentary Geology) Special Publication, Vol.69, p. 9 – 20.

Goldstein, R.H., 2003. Petrographic Analysis of Fluid Inclusions. Ch.2, in: Fluid Inclusions Analysis and Interpretation, I. Samson, A. Anderson and D. Marshall, (eds.), Mineral. Assoc. Can., Short Course Ser., Vol.32, p. 9 – 53.

Hadi, A., Musa, E. and Al-Bassam, K.S., 2010. Genesis of copper-iron mineralization and the associated rocks in Waraz area, Northeast Iraq. International Journal for Sciences and Technology, Vol.5, No.4, p. 27 – 47.

Herron, M.M., 1988. Geochemical classification of terrigenous sands and shales from core or log data. J. Sediment. Petrol., Vol.58, No.5, p. 820 – 829.

Hoefs J., 2009. Stable Isotope Geochemistry. Springer-Verlag, Berlin. 293pp.

Ilbeyli, N., Pearce, J.A., Thirlwall, M.F. and Mitchell, J.G., 2004. Petrogenesis of collision-related plutonics in Central Anatolia, Turkey. Lithos, Vol.72, p. 163 – 182.

Jassim, S.Z. and Goff, C., 2006. Geology of Iraq. Published by Dolin, Prague and Moravian Museum, Brno, 341pp.

Kesler, S.E., 2005. Ore-Forming Fluids. Elements, Vol.1, No.1, p. 13 – 18.

Klein, C. and Hurlburt, C., 2002. Mineral Science. John Wiley and Sons. New York. 641pp.

Lufkin, J.L., 2010. Origin of Ore Textures: Porphyry Copper Deposits, Rocky Mountain. 62th Annual Meeting of Geological Society of America (GSA), Vol.42, No.3, 1pp.

Maheo, G., Bertrand H., Guillot S., Villa I.M., Keller F. and Copiez P., 2004. The South Ladakh ophiolites (NW Himalaya, India): An intraoceanic tholeiitic arc origin with implication for the closure of the Neo-Tethys. Chemical Geology, Vol.203, p. 273 – 303.

Mirza, T.A. and Rashid, S.Gh., 2018. Mineralogy, fluid inclusions and stable isotopes study constraints on genesis of sulfide ore mineral, Qala Diza area, Qandil Series, Iraqi Kurdistan Region, Arab. J. of Geosci., Vol.11, 146pp.

Mirza, T.A., Kalaitzidis, S.P., Mohammed, S.H., Rashid, S.Gh. and Petrou X., 2017. Geochemistry and genesis of sulphide ore deposits in Sharosh Village, Qandil Series, Kurdistan Region, NE Iraq, Arab. J. Geosci., Vol.10, 428pp.

Miyashiro, A. and Shido, F., 1975. Tholeiitic and calcalkaline series in relation to the behavior of Ti, V, Cr and Ni. Am. Jour. Sci., Vol.275, p. 265 – 277.

Moghadam, H.S. and Stern, R.J., 2011. Geodynamic evolution of Upper Cretaceous Zagros ophiolites: formation of oceanic lithosphere above a nascent subduction zone. Geological Magazine, Vol.148, p. 762 – 801.

Musa, E.O., 2007. Petrography, Geochemistry and Genesis of Copper-Iron Mineralization and Associated Rocks in Waraz Area, Sulaimaniyah, NE Iraq. Unpublished M.Sc. Thesis, University of Baghdad, Baghdad, 155pp.

Nahab, M.Y., Fattah, A.S., Saffo, J.K. and Mohammad, S.N., 1979. Complex geophysical investigation for copper mineralization at Mawat area. GEOSURV, int. rep. no. 938.

Nielsen, H., 1979. Sulfur isotopes. In: E. Jager and J. Hunziker (eds.), Lectures in Isotope Geology. Springer, Berlin, p. 283 – 312.

O'Neill, H.S.C. and Palme, H., 1998. Composition of the silicate Earth: implications for accretion and core formation. In: Jackson, I. (ed.) The Earth's Mantle: Composition, Structure and Evolution, Vol.1. The Ringwood. Cambridge University Press, Cambridge. p. 3 – 126.

Ohmoto, H., 1986. Stable isotope geochemistry of ore deposits. Rev Mineral Geochem., Vol.16, No.1, p. 491 – 559.

Ohmoto, H. and Rye, R.O., 1979. Isotopes of sulfur and carbon. In: Barnes, H.L. (ed.) Geochemistry of Hydrothermal Ore Deposits, 2nd ed., John Wiley and Sons, New York, p. 509 – 567.

Pearce, J.A., 1982. Trace elements characteristics of lavas from destructive plate boundaries. In: Thorpe, R.S. (ed.), Orogenic Andesites and Related Rocks, John Wiley and Sons, New York, p. 525 – 548.

Pearce, J.A. and Gale, G.H., 1977. Identification of ore deposition environment from trace element geochemistry of associated igneous host rocks. Geol. Soc. Lond. Spec. Publ., Vol.17, p. 14 – 24.

Pearce, J.A. and Norry, M.J., 1979. Petrogenesis implications of Ti, Zr,Y and Nb variations in volcanic rocks. Contrib. Min. Petrol., Vol.69, p. 33 – 47.

Pe-Piper, G., Tsikouras, B. and Hatzipanagiotou, K., 2004. Evolution of boninite and island arc theoliites in the Pindos Ophiolite, Greece. Geol. Mag., Vol.141, No.4, p. 455 – 469.

Ramdohr, P., 1980. The Ore Minerals and Their Intergrowths. 2nd ed. Vol. 1 and 2. International Series in Earth Sciences. Edited by Ingreson, D.E. Pergamon Press. Oxford. 1205pp.

Ramdohr, P., 1981. The Ore Minerals And Their Intergrowth. Pergamon Press., New York, 1202 pp.

Richards, J.P., Spell, T., Rameh, E., Razique, A. and Fletcher, T., 2012. High Sr/Y magmas reflect arc maturity, high magmatic water content, and porphyry Cu ± Mo ± Au. Potential: examples from the Tethyan arcs of Central and Eastern Iran and Western Pakistan. Econ. Geol., Vol.107, p. 295 – 332.

Roedder, E.W., 1958. Technique for the extraction and partial chemical analysis of fluid-filled inclusions from minerals. Econ. Geol., Vol.53, No.3, p. 235 – 269

Roedder, E.W., 1984. Fluid Inclusions. Mineral Soc. Am. Rev. Mineral., Vol.12, 644 pp.

Savov, I., Ryan, J., Haydoutor, I. and Schijf, J., 2001. Late Precambrian Bulkan-Carpathian ophiolite- a slice of the Pan-African ocean crust?: Geochemical and tectonic insights from the Tcherni Vrah and Deli Joran massifs, Bulgaria and Sebria. Jour. Volcano. Geotherm. Res. Vol.110, p. 229 – 318.

Scoates, J.S. and Mitchell, J.N., 2000. The evolution of troctolitic and high-Al basaltic magma in Proterozoic anorthosite plutonic suites and implications for the Voisey's Bay massive Ni-Cu sulfide deposit. Econ. Geol., Vol.95, p. 677 – 701.

Seal, R.R. II., 2006. Sulfur isotope geochemistry of sulfide minerals. Rev. Mineral Geochem., Vol.61, p. 633 – 677.

Sengör, A.M.C. and Yilmaz Y., 1981. Tethyan evolution of Turkey: A plate tectonic approach. Tectonophysics, Vol.75, p. 181 – 241.

Shafaii, M. H., Stern R. J. and Rahgoshay, M., 2010. The Dehshir Ophiolite (Central Iran): geochemical constraints on the origin and evolution of the Inner Zagros Ophiolitic Belt. Geological Society of America Bulletin, Vol.122, p. 1516 – 47.

Shervais, J.W., 1982. Ti-V plots and the petrogenesis of modern and ophiolitic lavas. Earth Planet. Sci. Lett. Vol.59, p. 101 – 118.

Silva, F.C., Chavet, A. and Faure, M., 1998. General features of the gold deposits in the Rio Itapicuru Greenstone belt (Rigb, NE Brazil), discussion of the origin, timing and tectonic model. Revista Barsileira de Geociencias, Vol.28, p. 377 – 390.

Smirnov, V.A. and Nelidov, V., 1962. Report on 1: 200 000 prospecting correlation of Sulaimaniyah, Chwarta, Penjwin area, carried out in (1962). GEOSURV, int. rep. no. 290.

Sun, S. and McDonough, W.E., 1989. Chemical and isotopic systematics of ocean basalt: Implications for mantle composition and processes. In Sauders, A.D. and Norry, M.J. (eds.), Magmatism in the Ocean Basins. Geol. Soc. Lond. Spec. Publ. Vol.42, p. 313 – 345.

Van Wagoner, N.A., Leybourne, M.I., Dadd, K.A., Baldwin, D.K, and McNeil, W., 2002. Late Silurian bimodal volcanism of Southwestern New Brunswick, Canada: Products of continental extension. Geol. Soc. Am. Bulletin, Vol.114, No.4, p. 400 – 418.

Vanecek, M., 1972. The principal metallogenic features of Iraq. Acta Universitatis Carolinne-Geologica, Vol.3, p. 237 – 252.

Wilson, M., 1989. Igneous Petrogenesis. Unwin Hyman Ltd. London. 466pp.

Xu, J.F., Castillo, P.R., Chen, F.R., Niu, H.C., Yu, X.Y. and Zhen, Z.P., 2003. Geochemistry of Late Paleozoic mafic igneous rocks from the Kuerti area, Xinjiang, Northwest China: Implications for back-arc mantle evolution. Chem. Geol., Vol.193, p. 137 – 154.

Yara, I. and Mohammad, Y., 2018. Iron-copper mineralization associated with metagabbro in Mirawa Village, Kurdistan Region, Northeastern Iraq, Journal of Zankoy Sulaimani, Vol.20, No.2, p. 95 – 108.

Yassin, A.T., Alabidi, A.J., Hussain, M.L., Al-Ansari, N. and Knutsson, S., 2015. Copper ores in Mawat Ophiolite Complex (Part of ZSZ), NE Iraq. Natural Resources, Vol.6, p. 514 – 526.

Zhang, Z., Mao, J., Paul, R.T., Mei, F.Z., Zao, G., Yang, J., Wang, Z. and Zhang, Z., 2003. The Aoyougou mafic-ultramafic complex in the North Qilian Mountains, Northwest China: A possible middle Proterozoic ophiolite along the southern margin of the North China Craton. International Geology Review. Vol.45, p. 1 – 16

About the author

Dr. Irfan O.M. Yara, Lecturer at the University of Sulaimani, Iraq. He teaches undergraduate and postgraduate. Yara received his B.Sc. in geology from Sulaimani University, Iraq (2002) and M.Sc. degree in Petrology from the University of Baghdad in 2007, he got his Ph.D. degrees in Geochemistry and Ore Geology from TU Bergakadimie Freiberg – Germany in 2014. He taught in University of Kurdistan Hawler (2015 – 2018) as visiting lecturer. Yara published about 8 papers in petrology, ore mineralization, mineralogy and geochemistry in Iraqi and regional journals.

e-mail: irfan.mosa@univsul.edu.iq